Hindawi
Journal of Control Science and Engineering
Volume 2023, Article ID 5813277, 17 pages
https://doi.org/10.1155/2023/5813277

Research Article

Research on Reactive Power Optimization Control Method for Distribution Network with DGs Based on Improved Second-Order Oscillating PSO Algorithm

Youming Cai, Jingmin Liu, and Ning Gao

Logistics Engineering College, Shanghai Maritime University, Shanghai 201306, China

Correspondence should be addressed to Youming Cai; ymcai@shmtu.edu.cn

Received 7 April 2023; Revised 25 June 2023; Accepted 1 July 2023; Published 12 July 2023

Academic Editor: Petko Petkov

With the increasing penetration of distributed generation (DG) in the distribution network, the original network structure of the distribution network has been changed. In addition, the randomness and intermittency of renewable power generation will also have an impact on the voltage and power flow of the distribution network. To solve this problem, this paper proposes a reactive power optimization control method for distribution network with DGs based on second-order oscillating particle swarm optimization (PSO) algorithm with a constriction factor. Considering the economic operation of the distribution network, the proposed control method realizes the coordinated operation of the DGs and battery group with the conventional static reactive power compensation device, so as to improve the voltage quality of the distribution network and reduce the system network loss. At the same time, an improved second-order oscillating PSO algorithm is proposed to improve the speed and convergence of the multiobjective algorithm. Finally, the effectiveness of the proposed control method is verified by using MATLAB/Simulink on IEEE 33 bus distribution network with DGs in both static and dynamic situations.

1. Introduction

With the rapid increase of traditional fossil energy consumption and the increasingly serious environmental pollution, countries around the world have begun to develop and utilize renewable energy. DG integration into the distribution network can effectively reduce carbon emissions and achieve efficient use of renewable power generation. In practical operation, however, distributed DGs often have characteristics such as intermittent and uncertain power supply, and the integration of DGs into the distribution network will affect the magnitude and direction of the original power grid flow, resulting in a decrease in local voltage quality of the distribution network, increasing system losses, and significantly reducing the overall power supply reliability of the distribution network. With the continuous increase of grid-connected capacity of DGs, its impact on voltage quality and system network loss will become increasingly serious. Therefore, precise reactive power optimization models and efficient control algorithms for distribution networks containing DGs are of great importance. This has significant theoretical value and practical significance for optimizing the overall scheduling of distribution networks containing DGs, improving the voltage quality of distribution networks, and reducing their operating costs.

The conventional distribution network mainly has the following characteristics [1]. (1) The structure is radial. There is only one feeder between a single node and the power supply. (2) Energy flows unidirectionally. Due to the radial grid structure, the direction of electric energy only flows from the distribution transformer to the load node. (3) The power control capability is limited. The quantity of controllable devices is limited in the distribution network, so the operation state of the network varies less. With the integration of a large number of distributed power sources into the distribution network, the structure and operation mode of the power system at the medium and low voltage level will be changed, and the characteristics of the distribution network will also be

changed. The main effects are as follows [2]. (1) DG always has the characteristics of intermittence and uncertainty, and the integration of DGs into the distribution network will change the magnitude and direction of the power flow of the original distribution network, resulting in the decrease of the local voltage quality of the distribution network and increasing the system network loss. (2) Electricity supply does not match demand in time and space, which leads to energy waste and brings great challenges to the stable operation of the power grid. (3) The demand of distribution network for regulation ability is further increased to adapt to the structural transformation and the uncertainty of power flow.

The conventional distribution network normally regulates the voltage through transformers and reactive power compensation equipment. Choi and Kim [3] proposed to control the node voltage by changing the tap of the on-load tap changer, but the adjustment ability of this scheme to the terminal node of the distribution network is very limited, which is only suitable for the situation where the system reactive power can be balanced or has a certain reserve. Elrayyah et al. [4] pointed out that the most widely used method of regulating voltage in distribution network is to add reactive power compensation devices. However, the voltage regulation of conventional reactive power compensation device has certain regional limitations and improves the investment and maintenance cost.

With the integration of DGs, the reactive power and voltage optimization of distribution network are gradually complicated. On the one hand, more electronic converters make the number of adjustable reactive power supply in the distribution network increase greatly [5]. On the other hand, the intermittence and uncertainty of renewable power generation lead to the increase of power flow complexity of distribution network and the decrease of the regularity of node voltage characteristics, which also leads to the complexity of reactive power and voltage optimization control [6].

In the last few years, a lot of efforts have been made to demonstrate how the voltage optimization can be implemented in distribution systems [7]. On the one hand, some researches proposed to improve voltage quality from the perspective of picking the appropriate place and size of DGs. In [8], an optimal method of sizing and placement of DGs and distribution static synchronous compensator in the radial distribution network was proposed to lower active power losses, enhance voltage stability and profile, and minimize costs. In [9], a hybrid analytical and metaheuristic optimization technique is proposed to find the proper locations and sizes for the DG and distribution static synchronous compensator in distribution networks to minimize the total losses and improve the voltage profile. On the other hand, the voltage quality of distribution network with DGs is improved by advanced optimal control methods. In [10], the central controller was used to optimize parameters of piecewise linear functions and control the power output of PV units. In [11], the reactive power of DGs is controlled locally according to a piecewise linear static V-Q characteristic, and the central controller computes the reactive power regulation based on model predictive control. Considering the uncertainties of DG units and demand, a robust constrained model predictive control was proposed for voltage control in [12]. In [13], a particle swarm optimization (PSO) algorithm was used to solve the multiobjective mixed-integer nonlinear programming problem. In [14], an MPC-based framework was proposed to realize the local control of DG units, and the alternating direction method of multipliers algorithm was adopted to obtain the near-global optimization of voltage control. In [12], considering uncertainties from DG units and demands, a robust constrained model predictive control strategy was formulated for centralized voltage control. In [15], a two-stage voltage control strategy was proposed to coordinate DG units and OLTC. First, the OLTC operation is scheduled, and then the reactive power outputs of DG units are controlled. In [16], a new successive linear approximation method was proposed to handle the nonlinearity of the power flow equations, and then the reactive power optimal dispatch problem was solved by it. In [17], a data-driven stochastic reactive power optimization model was introduced to address uncertain DGs integrated into distribution networks. In [18], a power flow coordination and optimization control method based on deep reinforcement learning for power grid with DGs was proposed. In [19, 20], optimal distributed control strategies based on alternating direction method of multipliers and distributed MPC were proposed, which reduce the voltage deviation by optimizing the reactive power output of DGs. In [13], a PSO algorithm was used to solve the multiobjective mixed-integer nonlinear programming problem. From the references, the multiobjective optimization technique is commonly used to optimize the voltage of distribution network, while various solving methods for multiobjective optimization often face problems such as difficulty in convergence and inability to find a global optimal solution. In this paper, a reactive power optimization control method for distribution network with DGs based on an improved second-order oscillating particle swarm optimization algorithm is proposed.

The main research results and contribution of this paper are as follows. (1) The power output mathematical models of the photovoltaic system, wind turbine, and battery energy storage are established. (2) The influence of DGs on voltage is analysed, and a reactive power optimization mathematical model is established to minimize the network loss and node voltage deviation of the distribution network. (3) The inherent defects of the standard PSO algorithm are analysed from the perspective of control, and a second-order oscillating PSO algorithm with constriction factor is proposed to solve the reactive power optimization problem of distribution network with DGs. (4) An IEEE 33 bus distribution network model with DGs is simulated and analysed in static and dynamic scenarios. Simulation results confirm the performance and correctness of the proposed control method. With the proposed control methods, the convergence speed and optimization effect of reactive power optimization in distribution network with DGs are improved.

2. The Mathematical Model of Renewable Power Output

2.1. Photovoltaic Power Output Mathematical Model. With the inverter control, the photovoltaic power generation system can be regarded as the reactive power compensation equipment of the distribution network under the condition

that the inverter capacity is empty and participates in the reactive power optimization of the distribution network. Figure 1 shows the equivalent circuit of the photovoltaic power generation system.

Assuming that the external power grid is an ideal three-phase symmetrical voltage source, ignoring the influence of coupling inductance and distributed parameters, one of the phases is taken for analysis. The external grid voltage U_s is set as the reference voltage, that is, $\dot{U}_s = U_s\angle 0$; the output voltage U_{PV} of the photovoltaic inverter is set to $\dot{U}_{PV} = U_{PV}\angle\delta$, where δ is the angle between the photovoltaic inverter voltage and the grid voltage; ignoring the line resistance R, the current I on the line is

$$\dot{I} = \frac{U_{PV}\cos\delta + j\cdot U_{PV}\sin\delta - U_s}{jX} = \frac{U_{PV}\sin\delta}{X} + j\frac{U_s - U_{PV}\cos\delta}{X}. \tag{1}$$

The power provided by the photovoltaic power generation system to the grid is as follows:

$$\widetilde{S}_{PV} = P_{PV} + jQ_{PV} = \dot{U}_s\cdot\dot{I}^* = \frac{U_sU_{PV}\sin\delta}{X} + j\frac{U_s\left(U_{PV}\cos\delta - U_s\right)}{X}. \tag{2}$$

In (2), $\widetilde{S}_{PV}$ represents the apparent power of photovoltaic inverter; P_{PV} and Q_{PV} represent the active and reactive power of the photovoltaic power generation system, respectively.

In the distribution network, the angle δ between the output voltage of the photovoltaic inverter and the grid voltage is generally negligible, so it can be approximated as

$$\begin{cases} \sin\delta = \delta, \\ \cos\delta = 1. \end{cases} \tag{3}$$

Thus, (2) can be approximately simplified as follows:

$$\begin{cases} P_{PV} = \dfrac{U_sU_{PV}\delta}{X}, \\ Q_{PV} = \dfrac{U_sU_{PV} - U_s^2}{X}. \end{cases} \tag{4}$$

The reactive power output capacity Q_{PV} of the photovoltaic power generation system is mainly limited by the apparent power capacity and active output of the photovoltaic inverter.

$$\begin{cases} -\sqrt{S_{PV,\max}^2 - P_{PV}^2} \le Q_{PV} \le \sqrt{S_{PV,\max}^2 - P_{PV}^2}, \\ 0 \le P_{PV} \le P_{PV,\max}, \end{cases} \tag{5}$$

in which $S_{PV,\max}$ is the maximum apparent power capacity of the photovoltaic inverter and $P_{PV,\max}$ is the maximum active power of the photovoltaic power generation system. The photovoltaic power generation system normally operates in the maximum power point tracking (MPPT) mode. If the power loss in the inverter is ignored, the output power of the solar panel can be considered as the output power of the photovoltaic inverter. At this time, the function of regulating Q_{PV} can be realized by inverter control. Also, the photovoltaic power station can be equivalent to the PQ node during the power flow calculation.

2.2. Double-Fed Induction Generator Power Output Mathematical Model. Since double-fed induction generator (DFIG) can realize the decoupling control of active and reactive power and has the flexible ability of reactive power regulation, it has become one of the most widely used wind turbines. Therefore, the wind power generation system in the distribution network studied in this paper adopts DFIG. The equivalent circuit diagram of DFIG is shown in Figure 2.

Ignoring the internal energy loss of the wind turbine, the total power output of DFIG to the grid is

$$\begin{cases} P_{WT} = P_M = P_s + P_r = (1-s)P_s, \\ Q_{WT} = Q_s + Q_c, \end{cases} \tag{6}$$

in which P_s and P_r represent the active power output of DFIG stator winding and rotor winding, respectively; s represents the slip rate; and Q_s and Q_c represent the reactive power output of the stator-side converter and grid-side converter, respectively.

Considering the maximum current constraint of the rotor winding, the reactive power regulation range of the DFIG stator-side converter is

$$\begin{cases} Q_{s\max 1} = -\dfrac{3U_s^{\,2}}{2X_s} + \sqrt{\left(\dfrac{3X_m}{2X_s}U_sI_{r\max}\right)^2 - \left(\dfrac{P_{WT}}{1-s}\right)^2}, \\ Q_{s\min 1} = -\dfrac{3U_s^{\,2}}{2X_s} - \sqrt{\left(\dfrac{3X_m}{2X_s}U_sI_{r\max}\right)^2 - \left(\dfrac{P_{WT}}{1-s}\right)^2}, \end{cases} \tag{7}$$

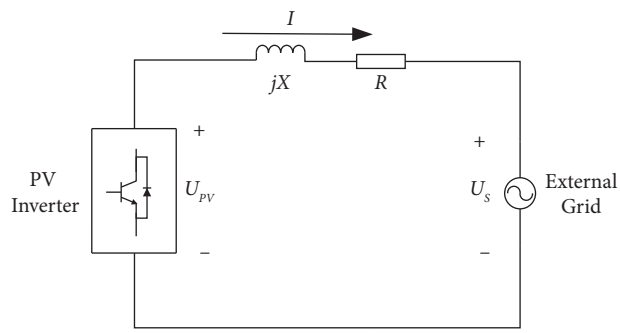

Figure 1: Equivalent circuit of the photovoltaic power generation system.

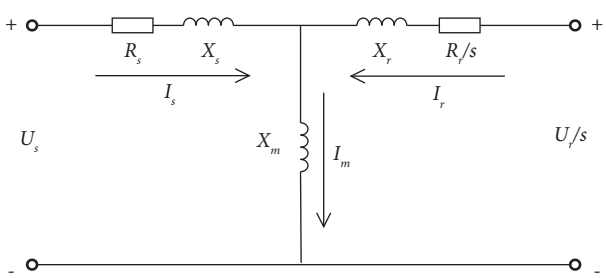

Figure 2: Equivalent circuit of DFIG.

in which U_s is the amplitude of DFIG stator winding voltage; X_s and X_m are the stator winding reactance and excitation reactance, respectively; and $I_{r\max}$ is the maximum value of DFIG rotor winding current.

Similarly, considering the maximum current constraint of the stator winding, the reactive power regulation range of the stator-side converter is shown in the following equation:

$$\begin{cases} Q_{s\max 2} = \sqrt{(U_s I_{s\max})^2 - \left(\dfrac{P_{WT}}{1-s}\right)^2}, \\ Q_{s\min 2} = -\sqrt{(U_s I_{s\max})^2 - \left(\dfrac{P_{WT}}{1-s}\right)^2}, \end{cases} \tag{8}$$

in which $I_{s\max}$ is the maximum value of DFIG stator winding current.

In summary, the reactive power regulation range of DFIG stator side is shown in the following equation:

$$\min\left(Q_{s\min 1}, Q_{s\min 2}\right) \le Q_s \le \max\left(Q_{s\max 1}, Q_{s\max 2}\right). \tag{9}$$

DFIG usually operates in constant power factor mode. When the wind speed is low, the grid-side converter of the wind turbine will operate in the under-excitation state, and the converter can participate in the reactive power regulation. The reactive power regulation capability of the DFIG grid-side converter is mainly limited by its maximum capacity. The reactive power regulation range of the DFIG grid side is as follows:

$$-\sqrt{S_{c\max}{}^2 - \left(\frac{sP_{WT}}{1-s}\right)^2} \le Q_c \le \sqrt{S_{c\max}{}^2 - \left(\frac{sP_{WT}}{1-s}\right)^2}, \tag{10}$$

in which $S_{c\max}$ is the maximum apparent power of the wind turbine grid-side converter and s represents the slip rate.

Therefore, the reactive power range of the DFIG output to the external grid is as shown in the following equation:

$$\begin{cases} Q_{WT\max} = Q_{s\max} + Q_{c\min}, \\ Q_{WT\min} = Q_{s\min} + Q_{c\min}. \end{cases} \tag{11}$$

2.3. Battery Energy Storage System Power Output Mathematical Model. The battery pack and inverter are important components of the battery energy storage system. Figure 3 shows the equivalent circuit of the grid-connected battery energy storage system, in which the energy storage system and the external main grid have the ability to supply power to the distribution network load. When the total active power output of DGs in the distribution network is greater than the total load of the distribution network, the battery pack is charged, so it can be equivalent to a load. When the total active power output of DGs in the distribution network is not enough to support the total load of the distribution network, the battery group discharges. At this time, the battery group is similar to photovoltaic and wind power and can be equivalent to a power source.

The charging and discharging amount of each period of battery energy storage is related to its own self-discharge rate and charging and discharging power. If the pulse characteristics of the battery pack are ignored, the state of charging of the adjacent period satisfies the following coupling relationship:

$$E_{BA}(t+1) = E_{BA}(t) \cdot (1-\sigma) + F_{\text{char}}\eta_c P_{BA}(t) - \frac{F_{\text{dis}} P_{BA}(t)}{\eta_d}, \tag{12}$$

in which $E_{BA}(t+1)$ and $E_{BA}(t)$ represent the remaining power of the battery energy storage in the $t+1$th and tth period, respectively; σ represents the self-discharge rate of the battery pack per hour; p_{BA} is the charging and discharging power of battery energy storage in the tth period; η_c and η_d represent the charging and discharging efficiency of battery energy storage, respectively; and F_{char} and F_{dis} represent the charging and discharging states of the battery pack at time t, which are variables of 0 or 1, respectively.

3. The Influence of DGs on Distribution Network

The integration of DGs into the distribution network will destroy the original single-source radial structure, and the power flow will also vary, which will affect the node voltage and network loss of the distribution network. In this paper, a simplified distribution network connected with DG is taken as an example to analyse the impact of DG on node voltage and network loss. The topology of the simplified distribution network is shown in Figure 4.

3.1. The Influence of DG on Voltage. The voltage drop of the power grid can be divided into longitudinal component and transverse component. In the ideal distribution network, the

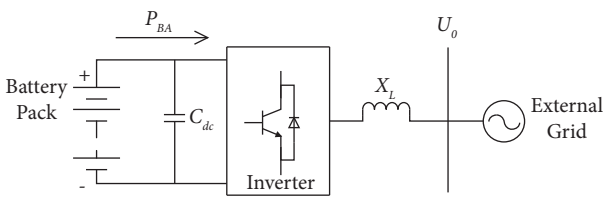

Figure 3: Equivalent circuit of grid-connected battery energy storage system.

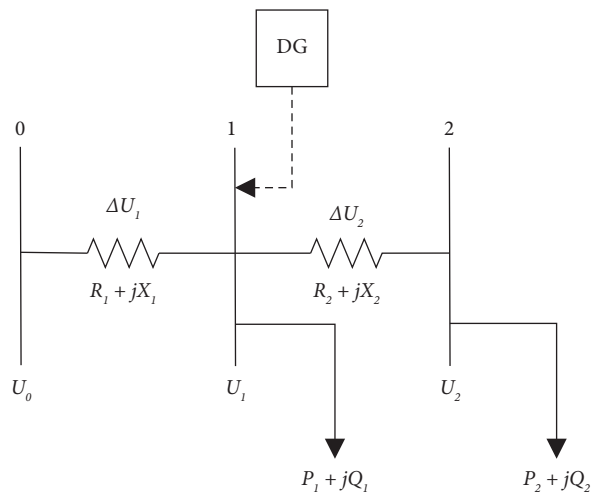

Figure 4: Topology of a simplified distribution network with DGs.

transverse component is generally ignored and only the influence of the longitudinal component of the voltage is considered [21]. The voltage drop is as follows:

$$\begin{cases} \Delta U_1 = \dfrac{P_1 R_1 + Q_1 X_1}{U_N}, \\ \Delta U_2 = \dfrac{P_2 R_2 + Q_2 X_2}{U_N}, \end{cases} \tag{13}$$

in which U_N represents the rated voltage of the distribution network. The total voltage drop of the distribution network is as follows:

$$\Delta U = \Delta U_1 + \Delta U_2. \tag{14}$$

The voltages at nodes 1 and 2 can be obtained:

$$\begin{cases} U_1 = U_0 - \Delta U_1 = U_0 - \dfrac{P_1 R_1 + Q_1 X_1}{U_N}, \\ U_2 = U_0 - \Delta U = U_0 - \dfrac{P_1 R_1 + P_2 R_2 + Q_1 X_1 + Q_2 X_2}{U_N}. \end{cases} \tag{15}$$

When a DG device reaches node 1 (as shown in the dotted line of Figure 4), the voltage loss ΔU_1 becomes

$$\Delta U_1' = \frac{(P_1 - P_{DG}) R_1 + (Q_1 - Q_{DG}) X_1}{U_N}, \tag{16}$$

in which P_{DG} and Q_{DG}, respectively, represent the active and reactive power of the DG device. Then, the voltage of node 1 and node 2 can be expressed as follows:

$$\begin{cases} U_1' = U_0 - \Delta U_1' = U_0 - \dfrac{(P_1 - P_{DG}) R_1 + (Q_1 - Q_{DG}) X_1}{U_N}, \\ U_2' = U_0 - \Delta U' = U_0 - \dfrac{(P_1 - P_{DG}) R_1 + P_2 R_2 + (Q_1 - Q_{DG}) X_1 + Q_2 X_2}{U_N}. \end{cases} \tag{17}$$

By comparing (15) and (17), it can be seen that the integration of DGs into the distribution network will increase the node voltage of the distribution network, and the increase of the node voltage is related to the power output of the DG device.

3.2. The Influence of DG on Power Loss. The integration of DG will also affect the system power loss, and the degree of influence varies with the power flow. In order to simplify the analysis process, assuming that the node voltage of the distribution network with the integration of DG remains unchanged, this paper only considers the steady states of the distribution network in Figure 4.

In the original distribution network, the power flow is unidirectional, and the current flowing into each load is

$$\begin{cases} I_{L1} = \dfrac{P_1 + jQ_1}{U_1}, \\ I_{L2} = \dfrac{P_2 + jQ_2}{U_2}. \end{cases} \tag{18}$$

The power loss on two feeders of the distribution network is as follows:

$$\begin{cases} \Delta S_1 = \Delta P_1 + j \cdot \Delta Q_1 = {I_{L1}}^2 \cdot (R_1 + jX_1), \\ \Delta S_2 = \Delta P_2 + j \cdot \Delta Q_2 = {I_{L2}}^2 \cdot (R_2 + jX_2), \end{cases} \tag{19}$$

in which ΔS_1 and ΔS_2 represent the line loss between nodes 0 and 1 and nodes 1 and 2, respectively. The total loss of the distribution network is as follows:

$$\Delta S = \Delta S_1 + \Delta S_2 = \frac{P_1^{\ 2} + Q_1^{\ 2}}{U_N^2} \cdot (R_1 + jX_1) + \frac{P_2^{\ 2} + Q_2^{\ 2}}{U_N^2} \cdot (R_2 + jX_2). \tag{20}$$

When a DG is integrated into node 1 and reaches the steady state, it injects active and reactive power into the distribution network, and the load current flowing into node 1 becomes

$$I_{L1}^{'} = \frac{(P_1 - P_{DG}) + j(Q_1 - Q_{DG})}{U_1}. \tag{21}$$

Thus, the line loss between nodes 0 and 1 becomes

$$\Delta S_1^{'} = \Delta P_1^{'} + j \cdot \Delta Q_1^{'} = I_{L1}^{'\ 2} \cdot (R_1 + jX_1). \tag{22}$$

The total loss of the distribution network with the integration of DG is as follows:

$$\Delta S^{'} = \Delta S_1^{'} + \Delta S_2 = \frac{(P_1 - P_{DG})^2 + (Q_1 - Q_{DG})^2}{U_N^2} \cdot (R_1 + jX_1) + \frac{P_2^{\ 2} + Q_2^{\ 2}}{U_N^2} \cdot (R_2 + jX_2). \tag{23}$$

By comparing (20) and (23), it can be seen that with the integration of DG, the network loss will change, and the total loss variation is closely related to the output of the DG.

4. Reactive Power and Voltage Optimal Control Method of Distribution Network Based on Improved Second-Order Oscillating PSO Algorithm

4.1. Reactive Power Optimization Mathematical Model of Distribution Network with DGs. The reactive power and voltage optimization control of the distribution network with DGs coordinates the reactive power output of the DGs and the conventional reactive power compensation device to achieve the purpose of reducing the system network loss stabilizing the voltage of each node and improving the economic operation ability of the distribution network. The control variables of the reactive power optimization mathematical model are the reactive power of the photovoltaic power station, the reactive power of the DFIG, the reactive power of the battery, and the reactive power of the static reactive power compensation equipment. The mathematical model consists of three parts: objective function, equality constraint equation, and inequality constraint equation.

4.1.1. Objective Function. In this paper, the system network loss and the voltage deviation of each node are taken as the optimization objectives, and the overlimit of each node voltage and the power purchase power from the superior power grid are added to the total objective function in the form of penalty function. The specific expression is as follows:

(1) Overall active power loss objective function:

$$f_1 = \min\left[\frac{\sum_{k=1}^{n} G_{ij}\left(U_i^{\ 2} + U_j^{\ 2} - 2U_i^{\ 2}U_j^{\ 2}\cos\theta_{ij}\right)}{P_{\text{loss}}}\right], \tag{24}$$

in which n represents the total number of branches in the distribution network; U_i and U_j represent the node voltage amplitude of i and j nodes, respectively; G_{ij} represents the conductance between i and j nodes; θ_{ij} represents the phase difference of node voltage between i and j nodes; and P_{loss} represents the network loss of the distribution network before optimization.

(2) Voltage deviation objective function:

$$f_2 = \min\left[\frac{\sum_{i=1}^{m-1}\left|U_i - U_0\right|}{\Delta U_{\text{sum}}}\right], \tag{25}$$

in which m represents the number of nodes in the distribution network; U_i represents the voltage amplitude of node i; U_0 represents the voltage amplitude of the balance node of the distribution network; and ΔU_{sum} represents the sum of voltage deviations of each node before optimization.

(3) Comprehensive objective function:

$$F = \min\left[\alpha \cdot f_1 + \beta \cdot f_2 + \lambda_1 \sum_{i=1}^{m} (U_i - U_{\text{lim}})^2 + \lambda_2 (P_{\text{in}} + Q_{\text{in}})\right], \tag{26}$$

in which U_{lim} represents the limit of the voltage amplitude of each node in the distribution network, and its value rules are as follows (calculated in per unit value):

$$U_{\text{lim}} = \begin{cases} 1.05, & (U_i \geq 1.05), \\ U_i, & (0.95 < U_i < 1.05), \\ 0.95, & (U_i \leq 0.95). \end{cases} \tag{27}$$

In the above objective function, α and β are the weight coefficients of the targets f_1 and f_2, respectively. In order to balance the influence of distribution network loss and voltage deviation, the values of α and β are 0.5; P_{in} and Q_{in} represent the active and reactive power purchased from the superior power grid, respectively. The reactive power

optimization model in this paper only considers the local consumption of DGs, regardless of the factors such as the distribution network selling electricity to the main grid. That is to say, the power can only flow from the main network to the distribution network in one direction, and the flow is irreversible. The penalty coefficient of the penalty function is expressed by λ_1 and λ_2, where λ_1 represents the penalty coefficient of the node voltage exceeding the limits and λ_2 represents the penalty coefficient of the power purchased from the main grid.

4.1.2. Equality Constraint. The equality constraint of the proposed reactive power optimization model in this paper is the power flow constraint equation of the distribution network, and its expression is as follows:

$$\begin{cases} P_{Gi} - P_{Li} = U_i \sum_{j=1}^{m} U_j \left(G_{ij} \cos\theta_{ij} + B_{ij} \sin\theta_{ij}\right), \\ Q_{Gi} - Q_{Li} = U_i \sum_{j}^{m} U_j \left(G_{ij} \sin\theta_{ij} - B_{ij} \cos\theta_{ij}\right), \end{cases} \tag{28}$$

in which P_{Gi}, P_{Gj}, Q_{Li}, and Q_{Lj} represent the active and reactive power of power supply and load of i and j nodes, respectively, and B_{ij} represent the susceptance between i and j nodes.

4.1.3. Inequality Constraint. In the reactive power optimization process, some variables need to be constrained. These variable constraints can be divided into two categories: control variable constraint and state variable constraint.

The control variable constraints in this paper include the upper and lower limits of the output of each DG and that of the grid-connected static VAR compensator (SVC) compensation capacity.

(1) Constraints of DG reactive power output:

$$Q_{DGi,\min} \le Q_{DGi} \le Q_{DGi,\max}, \quad (i = 1, 2, \ldots, s), \tag{29}$$

in which Q_{DGi} represents the reactive power output of the i_{th} DG; $Q_{DGi,\max}$ and $Q_{DGi,\min}$ represent the maximum and minimum reactive power output of the i_{th} DG, respectively; and s represents the number of DG in the distribution network.

(2) SVC compensation capacity constraints:

$$Q_{SVCi,\min} \le Q_{SVCi} \le Q_{SVCi,\max}, \quad (i = 1, 2, \ldots, t), \tag{30}$$

in which Q_{SVCi} represents the reactive power of the i_{th} SVC in the distribution network and $Q_{SVCi,\max}$ and $Q_{SVCi,\min}$ represent the upper and lower limits of the i_{th} SVC, respectively.

(3) Voltage amplitude constraints:

$$U_{i\min} \le U_i \le U_{i\max}, \quad (i = 1, 2, \ldots, m-1), \tag{31}$$

in which U_i represents the voltage amplitude of node i except the balance node and $U_{i\max}$ and $U_{i\min}$ represent the upper and lower limits of voltage amplitude of node i, respectively.

4.2. Multiobjective Optimization Method Based on an Improved PSO Algorithm. PSO, also known as bird swarm algorithm, has the advantages of fewer parameter settings, simple structure, and strong robustness. However, the standard PSO algorithm is easy to fall into the local optimal solution in the later period of iteration when the parameters are constant, which will produce the phenomenon of "prematurity" and lead to the decrease of convergence accuracy.

4.2.1. Mathematical Analysis of the Limitations of Standard PSO. In the standard PSO algorithm, the update of the particle velocity is only related to the position of the particle and the optimal value of the individual and the group at the previous moment, ignoring the influence of the change of the particle position on the update of the velocity, which leads to the effective information of each particle being not fully utilized. The relevant mathematical explanation is as follows.

In the iteration formula of the standard PSO algorithm [22], suppose $\varphi_1 = \text{rand1} \cdot c_1$ and $\varphi_2 = \text{rand2} \cdot c_2$, and then the velocity and position update formula of the standard PSO algorithm can be transformed into the following form:

$$\begin{cases} v_i^{(k+1)} = \omega \cdot v_i^{(k)} + \varphi_1 \cdot \left(P_{\text{best},i}^{(k)} - x_i^{(k)}\right) + \varphi_2 \cdot \left(G_{\text{best}}^{(k)} - x_i^{(k)}\right), \\ x_i^{(k+1)} = x_i^{(k)} + v_i^{(k+1)}. \end{cases} \tag{32}$$

When the individual and the group optimal values of the particle are determined, the velocity of the particle is only related to the rate of change in particle position. In the classical kinematic equation, the velocity expression of the i_{th} particle is shown in the following equation:

$$v_i^{(k+1)} = v_i^{(k)} + a_i \cdot \Delta t, \tag{33}$$

in which a_i represents the acceleration of the i_{th} particle and Δt represents the time interval, which is represented by an iteration. If the inertia coefficient ω is 1, the acceleration a_i can be expressed as

$$\begin{aligned} a_i = v_i^{(k+1)} - v_i^{(k)} &= \varphi_1 \cdot \left(P_{\text{brst},i}^{(k)} - x_i^{(k)}\right) \\ &+ \varphi_2 \cdot \left(G_{\text{best},i}^{(k)} - x_i^{(k)}\right) = \frac{d^2 x_i^{(k)}}{dk^2}. \end{aligned} \tag{34}$$

It can be seen that when the individual optimal value and the group optimal value are determined, the relationship between the particle position and the number of iterations is a second-order constant coefficient differential equation. The general solution of the equation can be obtained by solving the formula as follows:

$$x_i^{(k)} = C_1 \cdot \cos\left(\sqrt{\varphi_1 + \varphi_2} \cdot k\right) + C_2 \cdot \sin\left(\sqrt{\varphi_1 + \varphi_2} \cdot k\right), \tag{35}$$

in which C_1 and C_2 are two different constants.

Obviously, the position x of the particle is the value of the constant amplitude oscillation with the increase of the number of iterations k, which will fluctuate continuously in a fixed interval. Moreover, it leads to the inability of the particle position to effectively oscillate and converge, making the algorithm easy to fall into the local optimal solution. Therefore, the method to suppress the constant amplitude oscillation of each particle position with the number of iterations k will give a solution to the "premature" phenomenon.

4.2.2. Basic Principle of Second-Order Oscillating PSO. It can be seen from (32) that in the $k + 1_{\text{th}}$ iteration, the velocity of the particle is the composition of the velocity of the particle, the individual optimal velocity increment, and the group optimal velocity increment in the k_{th} iteration. If only the incremental part of the individual optimal speed is considered, (32) can be expressed as follows:

$$v_i^{(k+1)} = x_i^{(k+1)} - x_i^{(k)} = \varphi_1 \cdot \left(P_{\text{best},i}^{(k)} - x_i^{(k)}\right). \tag{36}$$

Its differential expression is

$$\frac{dx_i^{(k)}}{dk} = -\varphi_1 \cdot x_i^{(k)} + \varphi_1 \cdot P_{\text{best},i}^{(k)}. \tag{37}$$

Converting the complex frequency domain for analysis, the Laplace transform of (36) can be obtained:

$$s \cdot x_i(s) = -\varphi_1 \cdot x_i(s) + \varphi_1 \cdot P_{\text{best},i}. \tag{38}$$

Furthermore, (38) can be expressed as

$$\frac{x_i(s)}{P_{\text{best},i}} = \frac{\varphi_1}{\varphi_1 + s}. \tag{39}$$

Clearly, the optimal speed increment part of the individual is equivalent to a first-order inertial link with a time constant of 1, an inertial gain of φ_1, $P_{\text{best},i}$ as input, and $x_i(s)$ as output. Similarly, the optimal speed increment of the group is also equivalent to a first-order inertial link with a time constant of 1, an inertial gain of φ_2, $G_{\text{best},i}$ as input, and $x_i(s)$ as output. Therefore, the velocity increment of the standard PSO is actually composed of two first-order oscillation links with $P_{\text{best},i}$ and $G_{\text{best},i}$ inputs in parallel.

A second-order oscillating particle swarm optimization (SOOPSO) algorithm [23] is proposed by replacing the two first-order oscillating links with two second-order oscillating links. The algorithm simulates the change of particle velocity more accurately and improves the global search ability of PSO algorithm. After introducing the second-order oscillating link, the algorithm has a stronger global optimization ability at the initial period of iteration ($k < T/2$), which makes the algorithm oscillate and converge. In the later period iteration of the algorithm ($k \geq T/2$), it is necessary to strengthen the local optimization ability to make the algorithm converge gradually. The update formula of particle velocity changes as follows:

$$\begin{cases} \xi_1 < \dfrac{2\sqrt{\varphi_1} - 1}{\varphi_1}, \quad \xi_2 < \dfrac{2\sqrt{\varphi_2} - 1}{\varphi_2}, \quad \left(k < \dfrac{T}{2}\right), \\ \xi_1 \geq \dfrac{2\sqrt{\varphi_1} - 1}{\varphi_1}, \quad \xi_2 \geq \dfrac{2\sqrt{\varphi_2} - 1}{\varphi_2}, \quad \left(k \geq \dfrac{T}{2}\right). \end{cases} \tag{40}$$

4.2.3. Second-Order Oscillating PSO with Constriction Factor. In order to enhance the global convergence of the SOOPSO algorithm and further improve the optimization performance of the algorithm, this paper proposed a constriction factor χ to replace the inertia coefficient ω on the basis of the second-order oscillating PSO algorithm to achieve a better convergence effect. The mathematical iteration formula is as follows:

$$\begin{cases} v_i^{(k+1)} = \chi\left[v_i^{(k)} + \varphi_1\left[P_{\text{best},i}^{(k)} - (1 + \xi_1)x_i^{(k)} + \xi_1 x_i^{(k-1)}\right] + \varphi_2\left[G_{\text{best}}^{(k)} - (1 + \xi_2)x_i^{(k)} + \xi_2 x_i^{(k-1)}\right]\right], \\ x_i^{(k+1)} = x_i^{(k)} + v_i^{(k+1)}, \end{cases} \tag{41}$$

in which the constriction factor is

$$\chi = \frac{2}{\left|2 - \varphi - \sqrt{\varphi^2 - 4\varphi}\right|}, \tag{42}$$

in which φ represents the sum of two learning factors c_1 and c_2, and then the update formula of particle velocity becomes

$$v_i^{(k+1)} = \chi \cdot \left(v_i^{(k)} + c_1 \cdot \text{rand1} \cdot \left(P_{best,i}^{(k)} - x_i^{(k)}\right) + c_2 \cdot \text{rand2} \cdot \left(G_{best}^{(k)} - x_i^{(k)}\right)\right). \tag{43}$$

Compared with the inertia coefficient, the introduced constriction factor in the update formula of particle velocity can more effectively adjust the direction of velocity and enhance the regional search ability of PSO algorithm.

Figure 5 shows the flowchart of the improved second-order oscillating PSO. The specific implementation steps of the SOOPSO algorithm after replacing the constriction factor are as follows:

(1) Input the initial parameters of the algorithm, calculate the value of the constriction factor χ, and initialize the velocity and position of the particle swarm.

(2) Calculate and compare the fitness values of each particle according to equation (26) and select the individual optimal value and the group optimal value.

(3) Judge the current iteration number k and calculate the values of convergence coefficients ξ_1 and ξ_2 according to (40).

(4) The velocity and position of the $k+1_{th}$ iteration of the particle are calculated by the improved update formula (41).

(5) Calculate the fitness value of each particle after updating and recalculate the individual optimal value and the group optimal value of the population.

(6) Determine whether the termination condition is satisfied, and if it is satisfied, the calculation is terminated and output the result; if not, return to the third step to continue the iterative calculation until the termination condition is satisfied.

4.2.4. Performance Analysis of SOOPSO with Constriction Factor. In order to analyse the convergence performance of the SOOPSO algorithm with constriction factors, three classic benchmark optimization problems were selected for solving experiments, including unimodal functions, multimodal functions, and combination functions. Meanwhile, the experimental results were compared and analysed with the SOOPSO algorithm and the standard PSO algorithm with linear inertia coefficients. Among them, the number of particles for all three algorithms is set to 30, and the maximum number of iterations for the algorithm is set to 500. The learning factor for the SOOPSO algorithm with a constriction factor is $c_1 = c_2 = 2.05$. The range of inertia coefficient ω of the SOOPSO algorithm with linear inertia coefficient is [0.4, 1.2], and the range of learning factors c_1, c_2 is [0.4,2.05]. Inertia coefficient ω of standard PSO algorithm is 0.8, and learning factor $c_1 = c_2 = 2.05$.

(1) Sphere function:

$$f_1(x) = \sum_{i=1}^{d} x_i^2 \left(-5.12 \le x_i \le 5.12\right). \tag{44}$$

The sphere function is a typical continuous unimodal function, with a solution space of d dimension which is set to 20 in this paper. The global minimum value of the function is obtained at $(x_1, x_2, \ldots, x_d) = (0, 0, \ldots, 0)$. The distribution diagram of this function in two-dimensional form and the convergence curve obtained by applying three algorithms are shown in Figure 6.

As shown in Figure 6, the convergence speed and accuracy of the SOOPSO algorithm with constriction factor are better than those of the SOOPSO algorithm with linear inertia coefficient and the standard PSO algorithm in solving continuous unimodal functions.

(2) Rosenbrock function:

$$f_2(x) = \sum_{i=1}^{d-1} \left[100 \cdot \left(x_{i+1} - x_i^2\right)^2 + \left(x_i - 1\right)^2\right] \cdot \left(-10 \le x_i \le 10\right). \tag{45}$$

The Rosenbrock function is a multimodal function with multiple local minima, where the global minimum of the function is located at the parabolic valley $(x_1, x_2, \ldots, x_d) = (1, 1, \ldots, 1)$. However, even though this parabolic valley is relatively easy to find, it is still difficult to converge to the global minimum. The dimension d of the solution space was set to 20, and the distribution diagram of this function in two-dimensional form and the convergence curves solved by the three algorithms are shown in Figure 7.

From Figure 7(b), it can be seen that the convergence rates of the three algorithms are roughly similar, but only the SOOPSO algorithm with a constriction factor can converge to the global optimal solution, while the convergence accuracy of the SOOPSO algorithm with linear inertia coefficient is only second to that of the SOOPSO algorithm with a contraction factor. The standard PSO algorithm ultimately falls into the local optimal solution.

(3) Ackley function:

$$f_3(x) = -20 \exp\left(-0.2\sqrt{\frac{1}{d}\sum_{i=1}^{d} x_i^2}\right) - \exp\left(\frac{1}{d}\sum_{i=1}^{d} \cos\left(2\pi x_i\right)\right) + 20 + \exp(1). \tag{46}$$

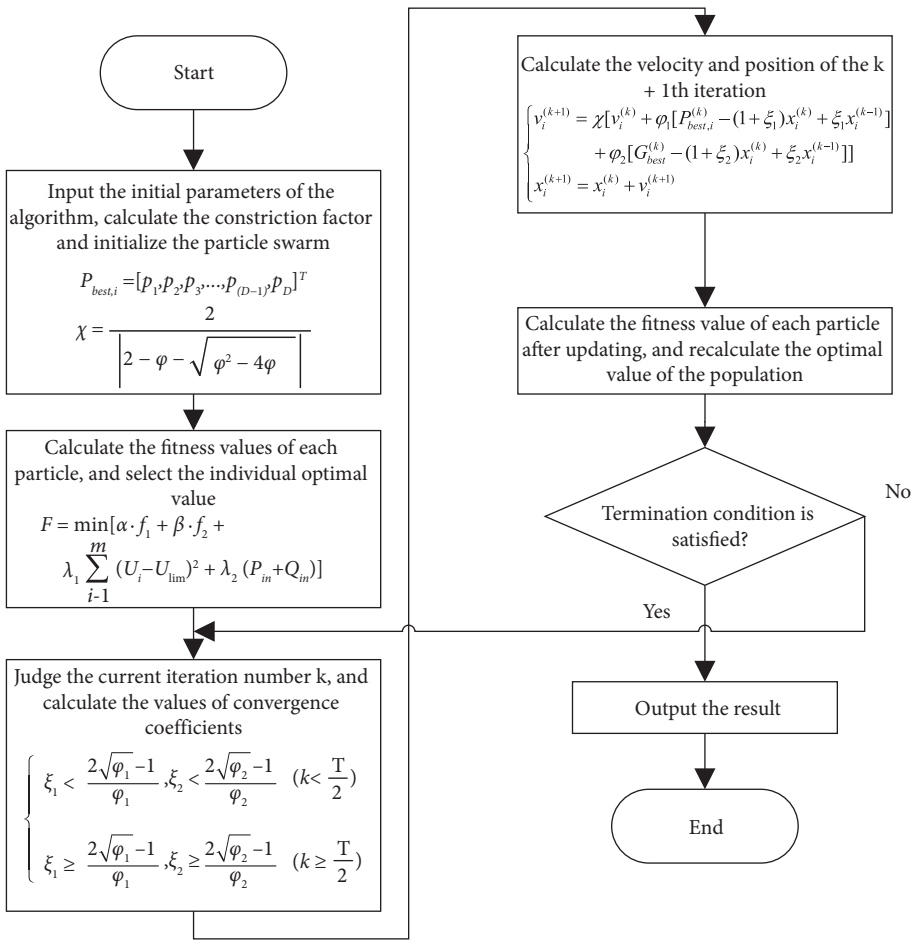

Figure 5: Flowchart of the improved second-order oscillating PSO.

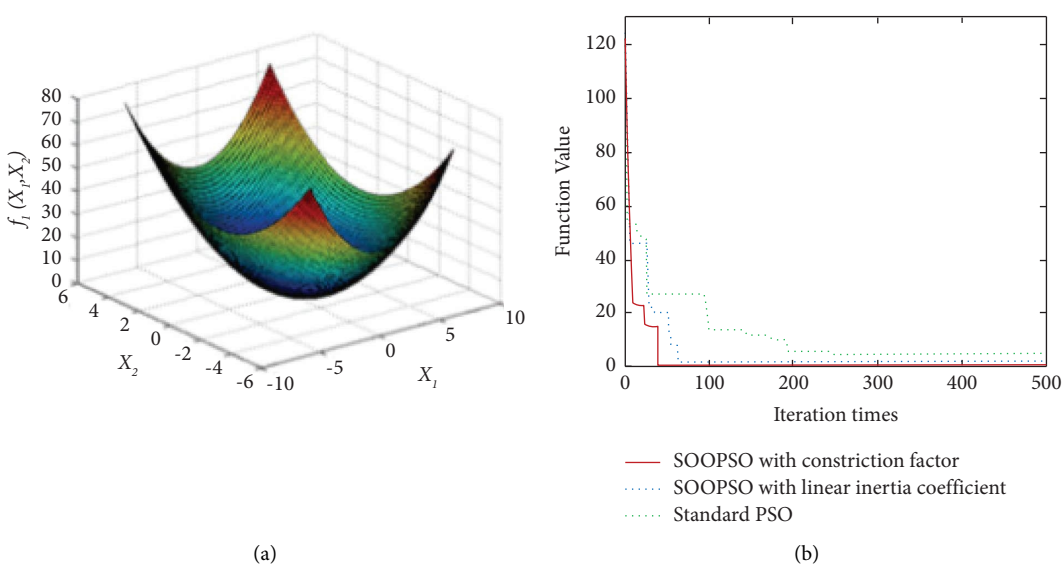

Figure 6: Function distribution diagram and convergence curve of sphere function. (a) Function distribution diagram. (b) Convergence curve.

The Ackley function has multiple local minima and a global minimum, which is obtained at $(x_1, x_2, \ldots, x_d) = (1, 1, \ldots, 1)$. This function can easily trap optimization algorithms such as hill climbing into many local optima and is widely used to test the ability of optimization algorithms to jump out of local optima. The search range of the algorithm

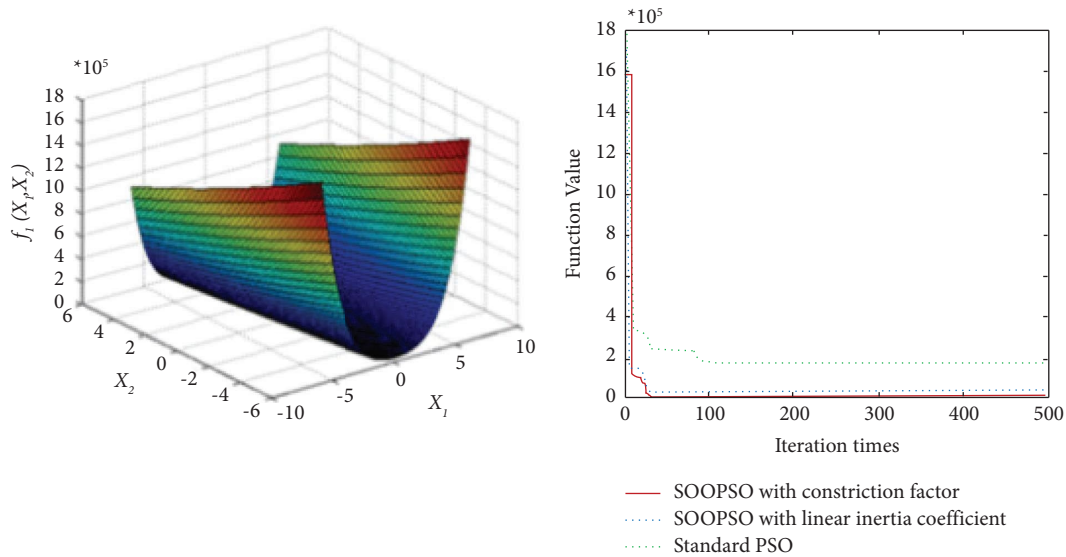

(a) (b)

Figure 7: Function distribution diagram and convergence curve of Rosenbrock function. (a) Function distribution diagram. (b) Convergence curve.

is set between [−32, 32], and the dimension d of the search space is 20. The two-dimensional distribution and convergence curves solved using the three algorithms are shown in Figure 8.

From Figure 8, it can be seen that compared to the other two algorithms, the SOOPSO algorithm with a constriction factor has the fastest convergence speed in the early stage and quickly jumps out of the local optimal solution to converge to the global optimal.

Through the experiments of the three test functions mentioned above, it can be found that the improved SOOPSO algorithm exhibits good optimization performance for both simple unimodal functions and complex multimodal functions. The convergence speed and accuracy of the algorithm are also better than those of the standard PSO algorithm and the SOOPSO algorithm with linear inertia coefficients.

5. Case Study

In order to verify the effectiveness of the proposed control method, this paper constructs a distribution network model containing DGs and battery packs on the basis of the standard IEEE 33 bus distribution network. Lithium storage battery packs with a rated capacity of 3.75 MWh are connected to node 6 and node 28, whose upper and lower limits of charge and discharge power are [−0.3 MW, 0.3 MW], and the self-discharge rate σ per hour is 0.01. Photovoltaic power stations with capacity of 0.8 MW and 0.05 MW are integrated to nodes 9 and 12, respectively. Wind turbines with capacity of 0.6 MW and 0.1 MW are integrated to nodes 17 and 19, respectively. The reference node of the system is 0 nodes, and the voltage reference is 12.66 kV. The reference value of the apparent power is 10 MVA. The total active power and reactive power of the distribution network load are 5084.26 kW and 2547.32 kvar, respectively. The topology of the IEEE 33 bus distribution network with integration of DG and SVC devices is shown in Figure 9. The simulation environment of this paper is AMD Ryzen5-4600 U CPU @ 2.10 GHz, 16.00 G memory, and the simulation software is MATLAB R2018b.

5.1. Reactive Power Optimization Effect in Steady State. According to the mathematical model of reactive power optimization obtained above, the reactive power optimization simulation in the steady state at a certain time is carried out. The active power of each distributed DG and battery pack is shown in Table 1.

The standard PSO, SOOPSO with linear inertia coefficient, and SOOPSO with constriction factor are used to simulate the case study. The parameters of the three algorithms are set as follows: the number of particles in the population is set to 50; the maximum number of iterations of the algorithm is 50; and the dimension of the search space is 8. In the standard PSO algorithm, the learning factor $c_1 = c_2 = 1.2$ and the inertia coefficient $\omega = 0.6$. In the SOOPSO algorithm with linear inertia coefficient, the learning factor $c_1 = c_2 \in [0.2, 1.8]$ and inertia coefficient $\omega \in [0.4, 0.9]$, which decrease linearly with the increase of iteration time. In the SOOPSO algorithm with contraction factor, the learning factor $c_1 = c_2 = 1.5$ and contraction factor χ are taken as in (41).

The steady-state simulation results with abovementioned reactive power optimization are shown in Table 2.

It can be seen from Table 2 that the system loss of the distribution network with DGs optimized by the three algorithms has decreased. Among them, the distribution network loss optimized by the SOOPSO algorithm with constriction factor is 0.1477 MW, which is 49.31% lower than that of pre-optimization, and is relatively lower than

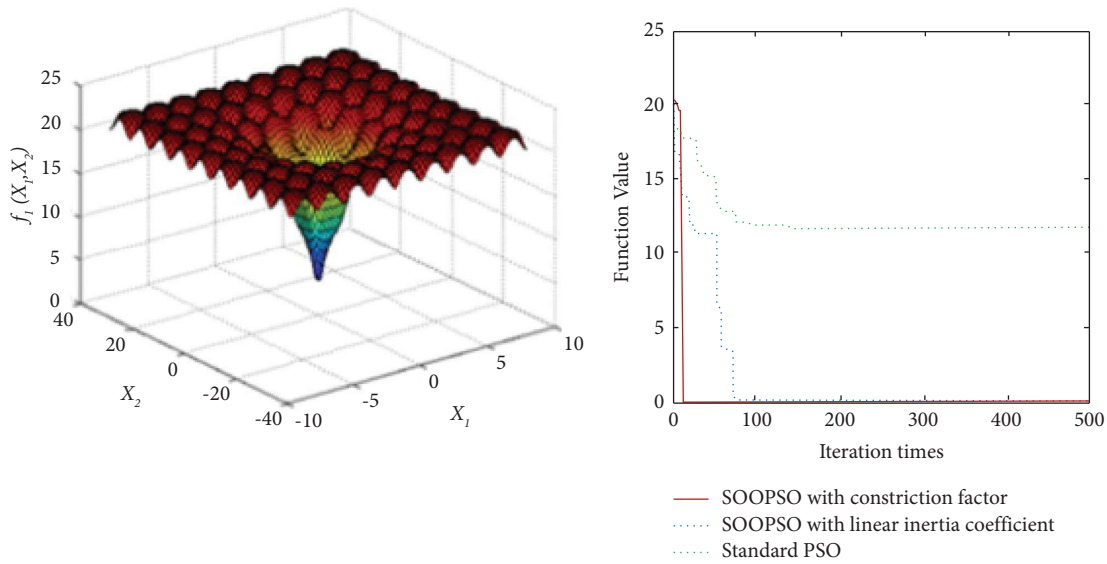

(a) (b)

Figure 8: Function distribution diagram and convergence curve of Ackley function. (a) Function distribution diagram. (b) Convergence curve.

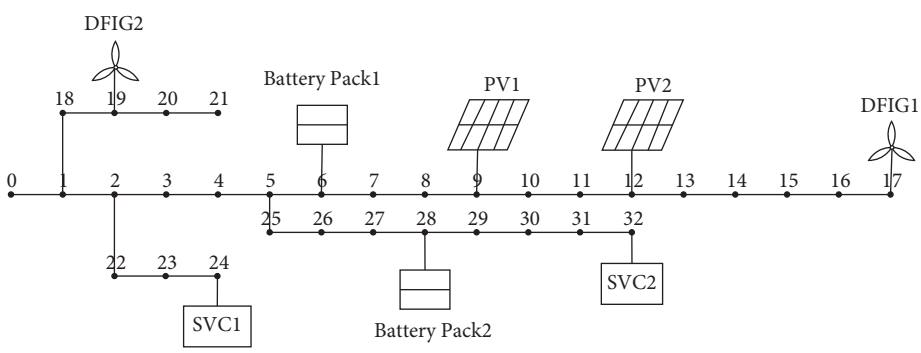

Figure 9: Topology of IEEE 33 bus with DGs integrated.

Table 1: Active power output of each equipment in the static distribution network.

Type of equipment	WT1	WT2	PV1	PV2	BA1	BA2
Node	17	19	9	12	6	28
Active power (MW)	0.3822	0.0570	0.4681	0.0200	0.1833	0.2367

Table 2: System loss simulation results in steady state.

Optimization method	System loss (MW)	Decrease rates (%)
Before optimization	0.1746	—
Standard PSO	0.0909	47.94
SOOPSO with linear inertia coefficient	0.0947	45.76
SOOPSO with constriction factor	0.0885	49.31

that of the other two algorithms. It can be seen that the SOOPSO algorithm with constriction factor has certain advantages in reducing system loss.

As shown in Figure 10, without reactive power optimization, the voltage of each node in the distribution network is generally low, especially nodes 17 and 32 at the end of feeders. The voltage amplitudes are 0.9467 and 0.9212, respectively, which are already lower than the limited node voltage lower limit of 0.95. After reactive power optimization, it can be seen that three algorithms can improve the node voltage to a certain extent, so that the overall voltage level is closer to the reference voltage. At the same time,

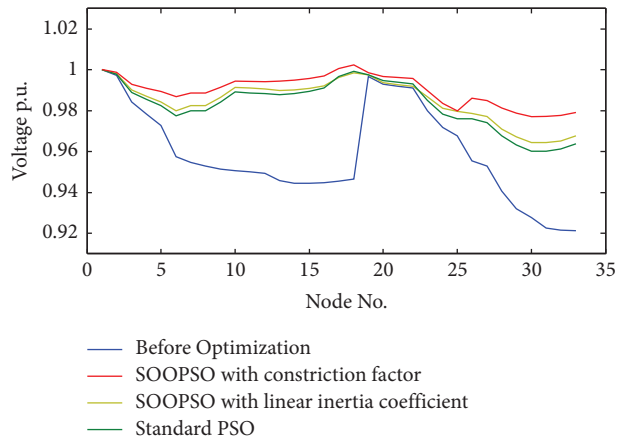

Figure 10: Node voltage simulation results in steady state.

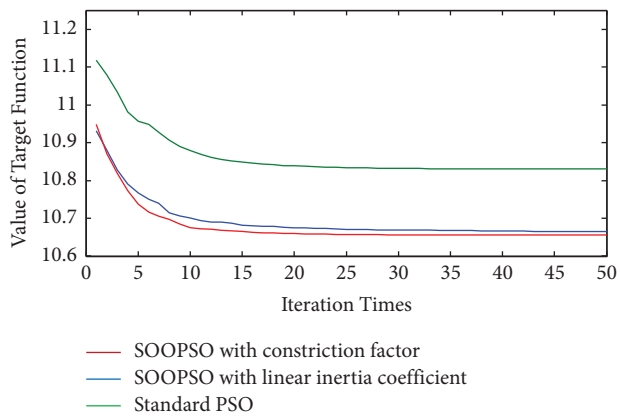

Figure 11: The convergence curves of three algorithms.

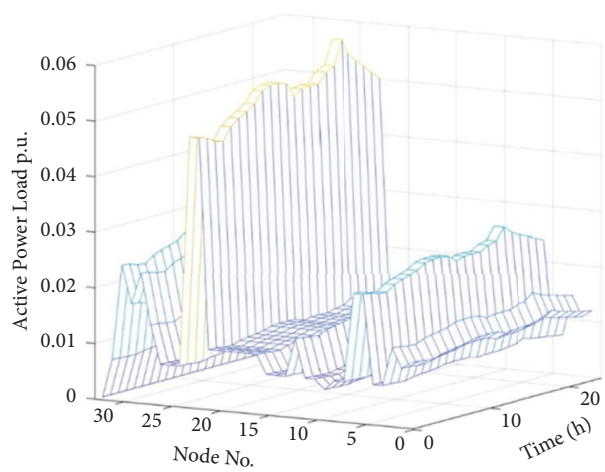

Figure 12: Active load of IEEE 33 bus distribution network.

among the three algorithms selected, the SOOPSO algorithm with constriction factor has the best optimization effect, and the voltage amplitude of each node does not exceed the limit. For nodes 17 and 32, the voltage amplitude optimized by the SOOPSO algorithm with constriction factor increases from 0.9467 and 0.9212 to 1.0100 and 0.9694, respectively.

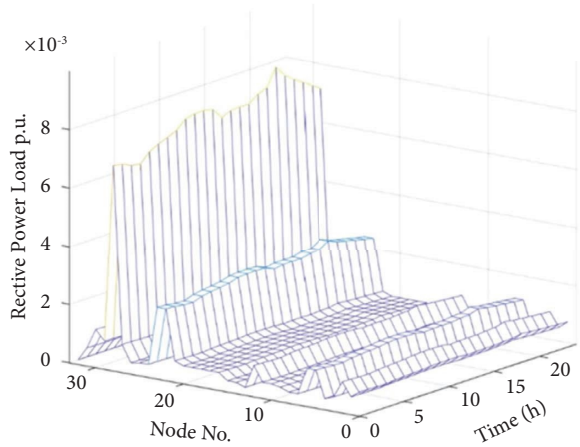

Figure 13: Reactive load of IEEE 33 bus distribution network.

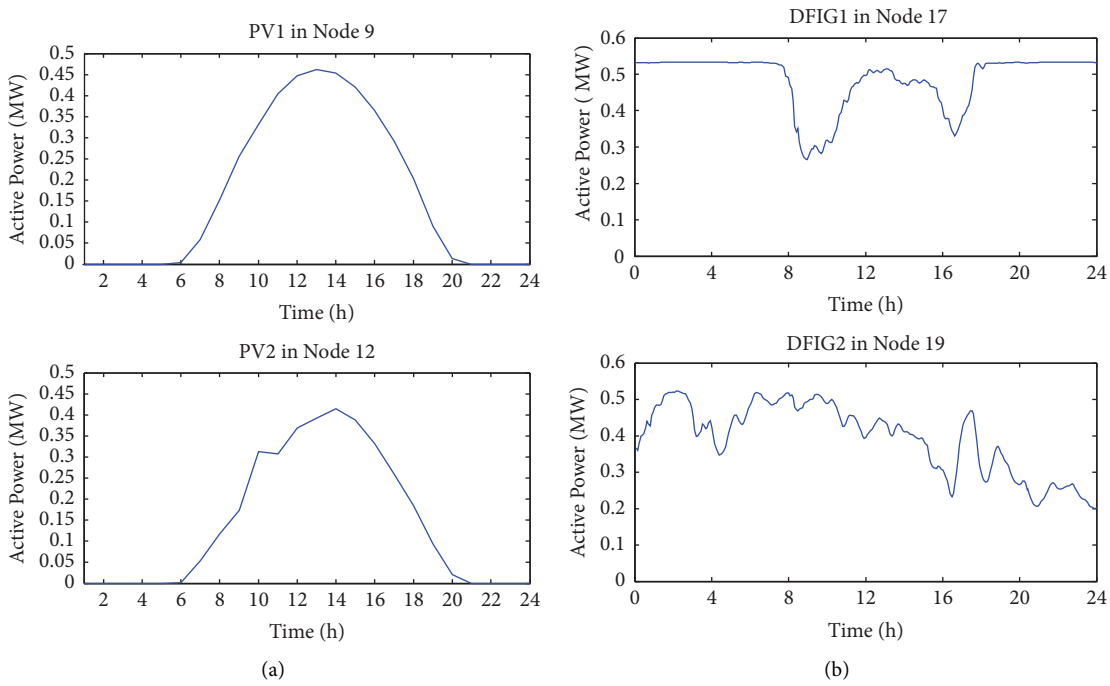

Figure 14: Continued.

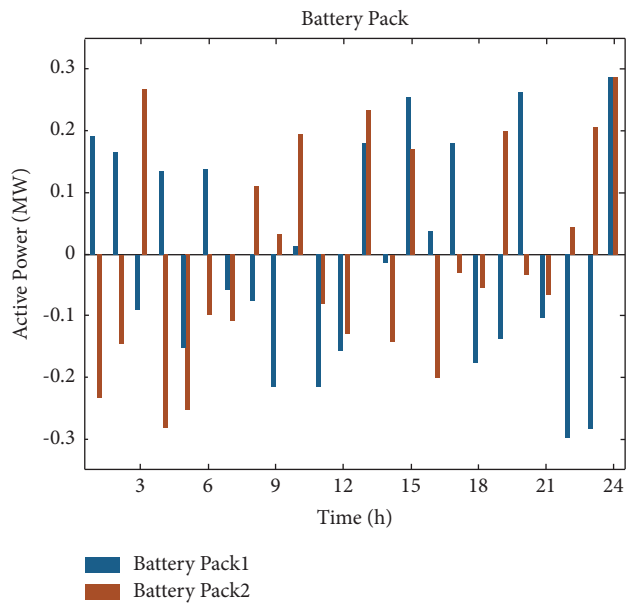

(c)

Figure 14: Active power of each DG and battery pack. (a) Power output of PV. (b) Power output of wind power. (c) Power output of battery pack.

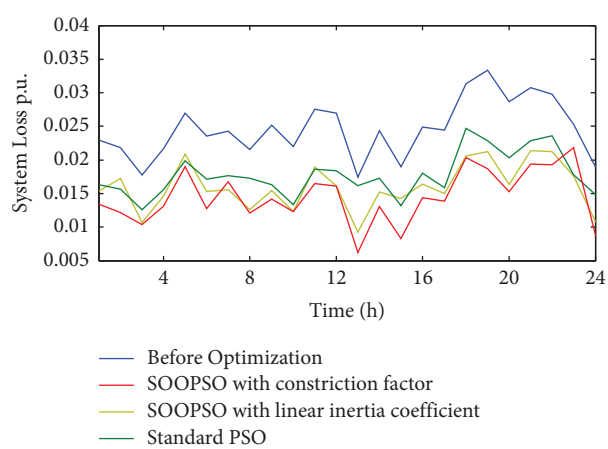

Figure 15: System loss under dynamic conditions.

Figure 11 shows the objective function convergence curves of reactive power optimization of three algorithms. It can be seen that the SOOPSO algorithm with constriction factor has better convergence speed.

5.2. Dynamic Reactive Power Optimization Effect. In order to verify the effectiveness of the proposed control algorithm in dynamic reactive power optimization, the simulation is carried out in one day, which is divided into 24 periods. Figures 12 and 13 show the active load and reactive load of each node in the IEEE 33 bus distribution network with DGs within 24 hours.

The active power of each DG and battery pack in the distribution network is shown in Figure 14.

After optimization, the network loss under dynamic conditions is shown in Figure 15 and Table 3. Compared with the other two algorithms, the SOOPSO algorithm with constriction factor has a better effect on reducing the network loss of the system.

Figure 16 shows the results of active power and reactive power purchased from the main grid. Table 4 shows the numerical analysis of simulation results. By optimization, both the active power and reactive power from the main grid are significantly reduced.

By comparing and simulating the results in both steady state and dynamic situation, the effectiveness of the SOOPSO algorithm with the constriction factor proposed in this paper is verified.

Table 3: Average system loss simulation results under dynamic conditions.

	Before optimization	SOOPSO with constriction factor	SOOPSO with linear inertia coefficient	Standard PSO
Average system loss (p.u.) in 24 h	0.0247	0.0136	0.0161	0.0189

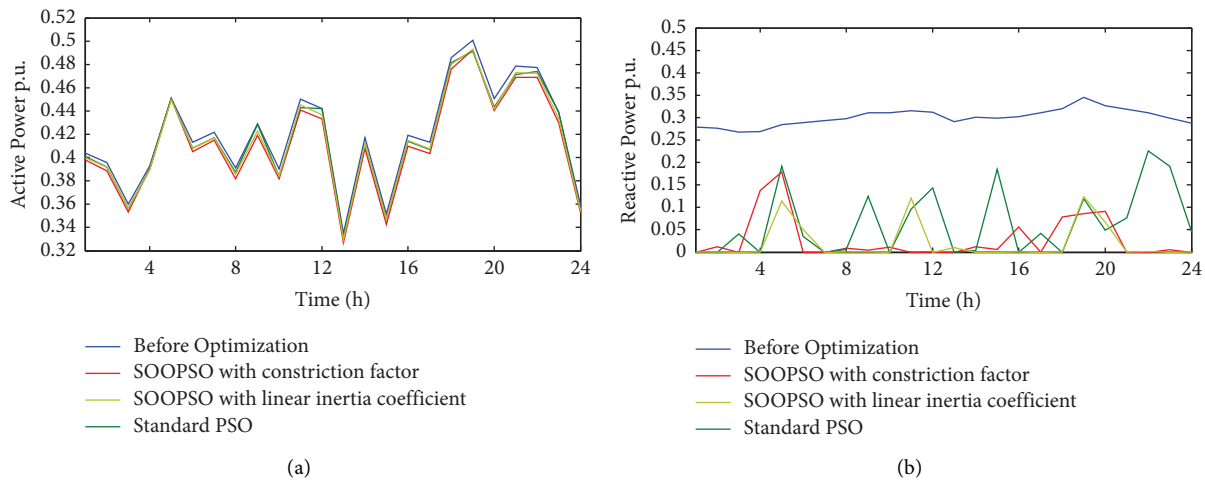

Figure 16: Simulation results of active and reactive power purchased from the main grid in each period. (a) Active power purchased from the main grid. (b) Reactive power purchased from the main grid.

Table 4: Average power purchased from the main grid.

	Before optimization	SOOPSO with constriction factor	SOOPSO with linear inertia coefficient	Standard PSO
Average active power purchased from the main grid	0.4362	0.4234	0.4289	0.4311
Average reactive power purchased from the main grid	0.3043	0.0678	0.0787	0.0989

6. Conclusion

This paper proposes a reactive power optimization control method for distribution network with DGs based on improved second-order oscillating PSO algorithm. The overall conclusion can be summarized in the following points:

(1) According to the simplified radial distribution network model, the influence of DGs on the node voltage and system loss of distribution network is analysed.

(2) A mathematical model of reactive power optimization for distribution network with DGs is established with the multiobjective of minimizing the active power loss and node voltage deviation.

(3) The inherent defects of the standard PSO algorithm are analysed from the perspective of control theory, and a SOOPSO algorithm with constriction factor is proposed, which can improve the convergence speed of PSO.

(4) The proposed control method is verified by the IEEE 33 bus distribution network with DGs under steady state and dynamic conditions. The simulation results show that the proposed SOOPSO algorithm with constriction factor has more advantages in convergence speed. Besides, it can effectively reduce the system network loss and node voltage deviation and improve the power supply stability of the distribution network with DGs.

Although this paper has done some research and discussion on reactive power optimization of distribution network with DGs, there are still some aspects that need to be further studied:

(1) In the next step, the reactive power output of DGs and static reactive power compensation device can be optimized in combination with real case simulation to improve the applicability of the model and algorithm.

(2) The reactive power compensation equipment in the case study only considers the static reactive power compensation device, and there are many kinds of reactive power compensation equipment in the current distribution network. Therefore, it can be considered to increase the switching capacitor, the on-load voltage regulating transformer, and the dynamic reactive power compensation device, so that the DGs can cooperate with a variety of reactive power compensation devices to further enrich the simulation examples.

Data Availability

The data used to support the findings of this study are available from the corresponding author upon request.

Conflicts of Interest

The authors declare that they have no conflicts of interest.

References

[1] A. Mohamed and T. J. T. Hashim, "Coordinated voltage control in active distribution networks," in *Electric Distribution Network Management Control*, pp. 85–109, Springer, Berlin, Germany, 2018

[2] N. Mahmud and A. Zahedi, "Review of control strategies for voltage regulation of the smart distribution network with high penetration of renewable distributed generation," *Renewable and Sustainable Energy Reviews*, vol. 64, pp. 582–595, 2016.

[3] J. H. Choi and J. C. Kim, "Advanced voltage regulation method of power distribution systems interconnected with dispersed storage and generation systems," *IEEE Transactions on Power Delivery*, vol. 16, no. 2, pp. 329–334, 2001.

[4] A. Y. Elrayyah, M. Z. C. Wanik, and A. Bousselham, "Simplified approach to analyzer voltage rise in LV systems with PV installations using equivalent power systems diagrams," *IEEE Transactions on Power Delivery*, vol. 32, no. 4, p. 1, 2016.

[5] H. Sun, Q. Guo, J. Qi et al., "Review of challenges and research opportunities for voltage control in smart grids," *IEEE Transactions on Power Systems*, vol. 34, no. 4, pp. 2790–2801, 2019.

[6] Y. P. Agalgaonkar, B. C. Pal, and R. A. Jabr, "Distribution voltage control considering the impact of PV generation on tap changers and autonomous regulators," *IEEE Transactions on Power Systems*, vol. 29, no. 1, pp. 182–192, Jan. 2014.

[7] M. E. Baran and I. M. El-Markabi, "A multiagent-based dispatching scheme for distributed generators for voltage support on distribution feeders," *IEEE Transactions on Power Systems*, vol. 22, no. 1, pp. 52–59, Feb. 2007.

[8] P. Zare, I. F. Davoudkhani, R. Zare, H. Ghadimi, and R. Mohajery, "Multi-objective optimization for simultaneous optimal sizing & placement of DGs and D-STATCOM in distribution networks using artificial rabbits optimization," in *Proceedings of the 2023 10th Iranian Conference on Renewable Energy & Distributed Generation (ICREDG)*, pp. 1–7, Shahrood, Iran, Islamic Republic of, March 2023.

[9] F. Fardinfar and M. J. K. Pour, "Optimal placement of D-STATCOM and PV solar in distribution system using probabilistic load models," in *Proceedings of the 2023 10th Iranian Conference on Renewable Energy & Distributed Generation (ICREDG)*, pp. 1–5, Shahrood, Iran, Islamic Republic of, January 2023.

[10] S. Weckx, C. Gonzalez, and J. Driesen, "Combined central and local active and reactive power control of PV inverters," *IEEE Transactions on Sustainable Energy*, vol. 5, no. 3, pp. 776–784, July 2014.

[11] H. S. Bidgoli and T. Van Cutsem, "Combined local and centralized voltage control in active distribution networks," *IEEE Transactions on Power Systems*, vol. 33, no. 2, pp. 1374–1384, Mar. 2018.

[12] S. Maharjan, A. M. Khambadkone, and J. C.-H. Peng, "Robust constrained model predictive voltage control in active distribution networks," *IEEE Transactions on Sustainable Energy*, vol. 12, no. 1, pp. 400–411, Jan. 2021.

[13] Y. J. Kim, J. L. Kirtley, and L. K. Norford, "Reactive power ancillary service of synchronous DGs in coordination with voltage control devices," *IEEE Transactions on Smart Grid*, vol. 8, no. 2, pp. 1–527, 2015.

[14] P. Li, J. Ji, H. R. Ji et al., "MPC-based local voltage control strategy of DGs in active distribution networks," *IEEE Transactions on Sustainable Energy*, vol. 11, no. 4, pp. 2911–2921, Oct. 2020.

[15] X. Sun, J. Qiu, and J. Zhao, "Real-time volt/var control in active distribution networks with data-driven partition method," *IEEE Transactions on Power Systems*, vol. 36, no. 3, pp. 2448–2461, May.2021.

[16] Z. Yang, A. Bose, H. Zhong, N. Zhang, Q. Xia, and C. Kang, "Optimal reactive power dispatch with accurately modeled discrete control devices: a successive linear approximation approach," *IEEE Transactions on Power Systems*, vol. 32, no. 3, pp. 2435–2444, May.2017.

[17] T. Ding, Q. Yang, Y. Yang, C. Li, Z. Bie, and F. Blaabjerg, "A data-driven stochastic reactive power optimization considering uncertainties in active distribution networks and decomposition method," *IEEE Transactions on Smart Grid*, vol. 9, no. 5, pp. 4994–5004, Sep. 2018.

[18] J. Kang, Y. Xu, B. Ding, M. Li, and W. Tang, "Power flow coordination optimization control method for power system with DG based on DRL," in *Proceedings of the 2023 5th Asia Energy and Electrical Engineering Symposium (AEEES)*, pp. 680–685, Chengdu, China, March 2023.

[19] P. Sulc, S. Backhaus, and M. Chertkov, "Optimal distributed control of reactive power via the alternating direction method of multipliers," *IEEE Transactions on Energy Conversion*, vol. 29, no. 4, pp. 968–977, Aug. 2014.

[20] G. Lou, W. Gu, Y. Xu, M. Cheng, and W. Liu, "Distributed MPC-based secondary voltage control scheme for autonomous droop-controlled microgrids," *IEEE Transactions on Sustainable Energy*, vol. 8, no. 2, pp. 792–804, Apr. 2017.

[21] A. R. Bergen and V. Vittal, *Power Systems Analysis*, Pearson Education, London, UK, 2006.

[22] E. Karunarathne, J. Pasupuleti, J. Ekanayake, and D. Almeida, "Optimal placement and sizing of DGs in distribution networks using MLPSO algorithm," *Energies*, vol. 13, no. 23, p. 6185, 2020.

[23] J. X. Hu and J. C. Zeng, "Two-order oscillating particle swarm optimization," *Journal of System Simulation*, vol. 19, no. 5, pp. 997–999, 2007.